# Structural Analysis of Ligand Protected Smaller Metallic Nanocrystals by Atomic Pair Distribution Function Under Precession Electron Diffraction

M. Mozammel Hoque,[1] Sandra Vergara,[1] Partha P. Das,[2] Daniel Ugarte,[3] Ulises Santiago,[1] Chanaka Kumara,[4] Robert L. Whetten,[1] Amala Dass,[4] and Arturo Ponce[*, 1]

[1]Department of Physics and Astronomy, University of Texas, San Antonio, Texas 78249, United States

[2]NanoMEGAS SPRL, Blvd Edmond Machtens 79, 1080 Brussels, Belgium

[3]Inst. de Física "Gleb Wataghin", Univ. Est. de Campinas-UNICAMP, CEP 13083-859, Campinas - SP, Brazil

[4]Department of Chemistry & Biochemistry, University of Mississippi, Oxford, MS 38677, United States

**ABSTRACT:** Atomic pair distribution function (PDF) analysis has been widely used to investigate nanocrystalline and structurally disordered materials. Experimental PDFs retrieved from electron diffraction (ePDF) in transmission electron microscopy (TEM) represent an attractive alternative to traditional PDF obtained from synchrotron X-ray sources, when employed on minute samples. Nonetheless, the inelastic scattering produced by the large dynamical effects of electron diffraction may obscure the interpretation of ePDF. In the present work, precession electron diffraction (PED-TEM) has been employed to obtain the ePDF of two different sub-monolayer samples —lipoic acid protected (~ 4.5 nm) and hexanethiolated (~ 4.2 nm, ~ 400-kDa core mass) gold nanoparticles—randomly oriented and measured at both liquid-nitrogen and room temperatures, with high dynamic-range detection of a CMOS camera. The electron diffraction data were processed to obtain ePDFs which were subsequently compared with PDF of different ideal structure-models. The results demonstrate that the PED-

ePDF data is sensitive to different crystalline structures such as monocrystalline (truncated octahedra) versus multiply-twinned (decahedra, icosahedra) structures of the face-centered cubic gold lattice. The results indicate that PED reduces the residual from 46% to 29%; in addition, the combination of PED and low temperature further reduced the residual to 23%, which is comparable to X-ray PDF analysis. Furthermore, the inclusion of PED resulted in a better estimation of the coordination number from ePDF. To the best of our knowledge, the precessed electron-beam technique (PED) has not been previously applied to nanoparticles for analysis by the ePDF method.

## INTRODUCTION

The atomic pair distribution function (PDF) approach has been widely used to investigate structurally disordered materials, because this method gives more detailed structural information compared with Bragg-peak based X-ray powder diffraction patterns.[1] PDF analysis can provide structural information not only in crystalline materials but also in short- and medium-range ordered materials; such as amorphous and nanostructured materials. This method provides insights about the degree of crystallinity, the atomic structure and size of the core region, atomic local environment, and the degree of the internal disorder.[2-3]

Traditionally, PDF is retrieved from X-ray diffraction data obtained on synchrotron beamlines and fit analyses are performed with several ideal structure-models to determine the most probable crystalline structure. Typically, a fit agreement factor *residual*, $R_w$, derived by least-squares approach (see results and discussion section for mathematical interpretation) defines the quality of the PDF with a value of ~ 0.2-0.3 (~ 20-30%), is considered to be an

acceptable fit agreement for structural analysis of gold and other noble metal nanoparticles,[4-10] although higher values are also reported. For example, Kumara *et al*.[11] performed PDF structural analysis of $Au_{\sim 940}(SR)_{\sim 60}$ (diameter ~ 3.3-nm; mass, ~ 200 kDa) using synchrotron X-ray data, reporting a $R_w$ = 44% for the comparison with a truncated octahedron (TOh) structure-model; whereas it appears, from inspection of the fit residual curve of their other work on the smaller compound $Au_{\sim 500}(SR)_{\sim 120}$ ( ~120 kDa)[12], that the decahedral (Dh) model is clearly superior.

The fitting process can be refined with strategies such as "cluster-mining", a method that uses many structure models instead of a unique model, with highly constrained refinement parameters to find the best structures for the specific nanoparticles.[13]

The structural analysis with X-ray diffraction (XRD) approach performed in synchrotron is regarded as a very powerful and reliable technique. However, this approach experiences a limitation that is critical at the nanoscale: the minimum amount of sample required is typically several milligrams, assuming a beam size ~ 100 μm - 1 mm for a reliable measurement. In this sense, PDF retrieved from electron diffraction measurements using a transmission electron microscope (TEM) presents an alternative approach to study nanocrystalline or structurally disordered materials. This approach permits the study of samples using quantities several orders of magnitude smaller than those required for synchrotron, reducing the amount of sample roughly from milligrams to the nanogram scale.

Nonetheless, the biggest issues encountered in the conventional electron diffraction technique are the large dynamical effects caused by the strong interaction of electrons with matter, and the beam damage that occurs after high electron doses. The electron dose may be dramatically reduced by using high dynamic-range detectors (CMOS camera), as described

below. However, the dynamical effects or multiple scattering interactions result in spurious reflections and non-proportional intensities in the electron diffraction patterns, which cannot be analyzed within the kinematical framework. Some alternative approaches to reduce these effects have been proposed (Blackman correction, for example);[14] however, this issue is still rather difficult to solve in a simple manner.

A significant reduction of dynamical effects can be achieved using precession electron diffraction (PED)[15], based on continually changing the beam orientation.[16-17] In PED the scanning coils deflect the electron beam so as to result in precession around a central point on the specimen plane. The origin of this technique started from Paul Midgley and Roger Vincent, who developed the diffraction technique to achieve quasi-kinematical scattering diffraction patterns to measure the intensities for crystalline structure determination.[17] Subsequently, Gjønnes demonstrated that experimental intensities obtained by PED must be corrected for geometrical factors analogous to the factors corrected for X-ray diffraction.[18]

The PED method has been employed not only to study the single crystals but also polycrystalline structures, e.g. hydroxyapatite nanopowders.[19-20] The integrated intensities of specific Bragg reflections for smaller metallic or polycrystalline-like nanoparticles are obtained from the profile of the Debye-Scherrer diffraction pattern.[21] The total intensity of the PED pattern from an ensemble of nanoparticles is an sum of the contribution from each particle, and will be reflected in the retrieved ePDF. Despite the fact that the ePDF method has been applied (since 2012) to analyze nanoparticles,[22] to the best of our knowledge it has not been previously applied to data obtained using the precessed electron beam **(**nanoparticle PED-PDF).

Note that the ePDF method does not require an expensive aberration-corrected TEM instrument, and the accessibility to a PED equipped TEM instrument also render these kinds of experiment easier and at a lower cost for the scientific community. When sample size and synchrotron beam time are available, X-rays will yield the best possible results for PDF structural analysis of nanoparticles. But a research project dealing with nano-objects may require more frequent studies than are convenient at an X-ray synchrotron beamline, in which case the PED-based PDF represents an invaluable approach to a research project as a whole, consisting of repeated synthesis, optimization, and characterization steps required to attain the final optimized nanostructure.

It is important to establish the advantages of the ePDF from the PED method for samples of different types, because these appeal to distinct audiences. Aqueous colloidal metal nanoparticles are investigated by a different community interested in biomedical applications, for example;[23-26] whereas, non-aqueous metallic nanoparticles are investigated for more fundamental research purposes.[11, 27-28] In this work, PDF analyses are carried out for aqueous phase lipoic acid (~ 4.5 nm) and non-aqueous phase hexanethiolate (~ 4.2 nm) protected Au nanoparticles (NPs) using PED; the results of ePDF from PED at room and low temperature (liquid-nitrogen) are compared. Finally, PDF fit analyses are performed with face-centered cubic (*fcc*), and multiple twin boundaries—icosahedron and decahedron—models of the observed structures in high resolution transmission electron microscopy (HRTEM) images.

## EXPERIMENTAL METHODS

*Synthesis of nanoparticles.* 4.5 nm Au NPs were synthesized using a solution of 2.2 mM trisodium citrate in 150 mL of ultrapure water (~18 MΩ) under vigorous stirring. Then, 0.1 mL of 2.5 mM tannic acid was added into the solution, followed by addition of 1 mL of 150 mM

potassium carbonate to adjust the pH of the solution (~11). The solution was heated under vigorous stirring; 1 mL of 28 mM $HAuCl_4$ was added at once as soon as the temperature of the solution reached ~ 68-69 ℃. The solution changed from transparent to turned dark gray instantaneously after gold precursor injection, and then to red wine color within 6-7 minutes, indicating the formation of very small Au NPs; the solution was kept at ~ 68 °C for 15 minutes to ensure complete reduction of the gold precursor. 1 mM solution of lipoic acid (LA), an important biological dithiolate, was prepared by adding NaOH (until LA completely dissolved) in 10 mL pure $H_2O$. Then 500 µL of this LA solution was added into 50 mL of as-synthesized Au NPs, and gently stirred overnight at room temperature to perform the ligand exchange reaction. To remove the unbound/unreacted or loosely connected ligands and other byproducts, nanoparticles were purified using a 10 kDa ultracentrifuge filter (MWCO 10000, Amicon) by centrifugation (10, 000 *rpm*, 6 minutes for filtering and 3 minutes for collecting filtered samples). Gold (III) chloride (99.99%), (trace metal basis) was purchased from Acros organics; trisodium citrate dihydrate (99%), potassium carbonate reagent (ACS anhydrous, 99%), tannic acid, and, HPLC grade ultrapure water were purchased from Alfa Aesar. All glassware was cleaned with aqua regia and rinsed with deionized water and acetone prior to use. Synthesis and characterization of the hexanethiolated Au NPs of ~ 4.2 nm is available in a separate article.[28]

*Electron microscopy.* Concentrated solutions of hexanethiolated Au NPs (~ 4.2 nm) or lipoic acid protected Au NPs (~ 4.5 nm) were drop casted on a commercial grid, LC300-Cu-100 (lacey carbon-copper grid, mess 300) thin carbon film (thickness ~ 5 nm). The nanoparticles solution was deposited only on half of the grid, and the uncovered region with carbon was used to acquire background diffraction patterns. The grid was mounted on a cryo-

TEM holder (Gatan 915) and diffraction patterns were obtained both at room and liquid-nitrogen (~ 90 K) temperatures.

TEM images and selected area electron diffraction (SAED) patterns were obtained on a JEOL 2010F microscope operating at 200 kV. Diffraction patterns were acquired in a highly sensitive 16-megapixel CMOS camera (TVIPS) with a dynamic range (maximum/noise) of 10,000:1 and images were registered at 16-bit to ensure the use of the maximum dynamic range of the camera (65,536 grayscale). Diffraction patterns are collected using camera lengths of 30 or 50 cm, an SAED aperture of 50 μm, and an exposure time of 1 s, the electron dose measured in the regions of interest was 8 e $Å^{-2}$ $s^{-1}$. We reported another method to analyze electron diffraction patterns using a methodology that prevents damage in metallic ligand-protected nanoparticles using higher electron doses combined with fast scanning electron diffraction.[29] In the present manuscript, we measure the electron diffraction patterns, without scanning, from a set of well distributed nanoparticles in larger field of views (***from 250000 to 640000 nm$^2$***) using low electron dose. The experimental set up consists of a precession electron diffraction unit (manufactured by Nanomegas) attached to the microscope that allows the collection of electron diffraction patterns under precession mode from 50 to100 Hz. The distortion introduced by camera length and precession angle was corrected during the imaging and mapping by the precession unit.[30] The precession angles used for the experiments were 8 or 25 mrad at 100 Hz. The intensity profiles of the electron diffraction patterns were obtained using radial diffraction ring profiler (version 1.2), DiffTools V5[31] plugins in Digital Micrograph software, and process diffraction software.[32-34] The recorded diffraction patterns were processed by centering each image, and subsequently subtracting the background of the amorphous carbon film (free of nanoparticles). Both diffraction patterns, background carbon

film and nanoparticles supported by it were acquired under exactly the same illumination condition for the acquisition of the diffraction patterns. The retrievals of the ePDF data were tested using three different programs: SUePDF,[35] eRDF,[36] and process diffraction software.[32-34] The fit agreement between experimental and simulated PDF functions is performed using DiffPy-CMI software.[37] The accuracy of the fitting is evaluated by the least-square residual,[4] $R_w$; which estimates the error between the theoretical and experimental PDFs.

## RESULTS and DISCUSSION

**TEM and Electron diffraction**. Figure 1 shows the narrow particle size distribution and the good dispersion of NPs in a carbon grid. Particle size distribution is measured by imageJ, image analysis software. Before measuring the size of the particles, a median filter is used for background subtraction. A series of diffraction patterns were collected at room temperature (RT) with and without precession consecutively, keeping same illumination conditions for both areas, with Au NPs and carbon film only; later on, liquid nitrogen was added to the cryo-TEM holder. When the temperature was stabilized at 90 K, a series of images were collected again, with and without precession.

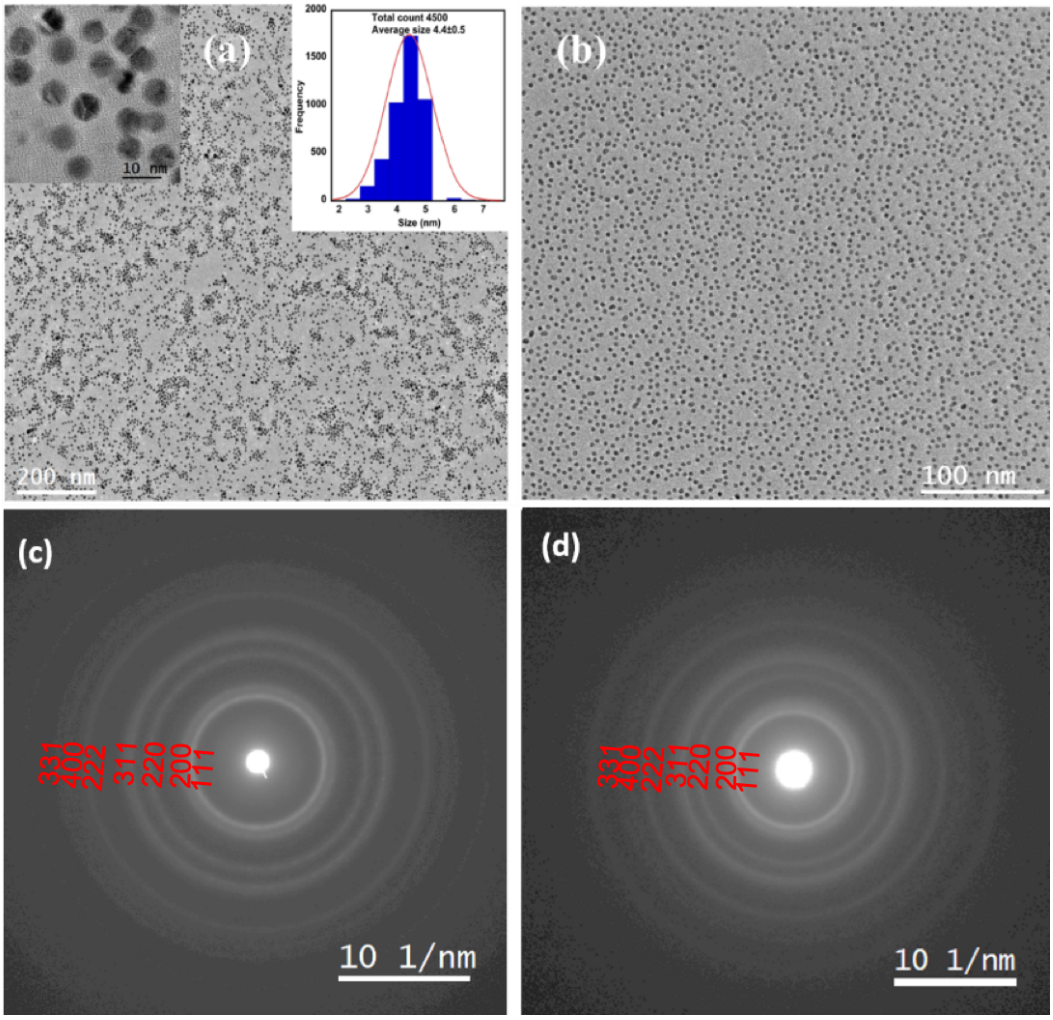


**Figure 1.** TEM images of lipoic acid and hexanethiolated Au NPs. (a) Low magnification TEM image of lipoic acid protected Au NPs. Inset showing particles size distribution profile (right side), and high-resolution images (left side); average size of the particles (4500 counts) ~ 4.4±0.5 nm. (b) TEM image of hexanethiolated Au NPs, average size of the particles ~ 4.2±0.4 nm. (c-d) Corresponding precession electron diffraction (cryo-PED) pattern of lipoic acid and hexanethiolated Au NPs, respectively; labels refer to indexing of major reflections, i.e. (111), (200), (220). Figure 1(c) has been acquired on camera length 50 cm, whereas (d) on camera length 30 cm.

Figure 2 shows the intensity profile after carbon (background) subtraction for the four conditions analyzed herein. In general, the signal-to-noise ratio improved with the use of

cryogenic conditions as well as the sharpening of the peaks. The inclusion of precession resulted in a reduction of spurious peaks in the high-$Q$ region, which are excessive oscillatory artifacts produced by the dynamical effects. For low-$Q$ scattering signal, it is less critical since the peaks contain very little information contributing the total local structure.[4]

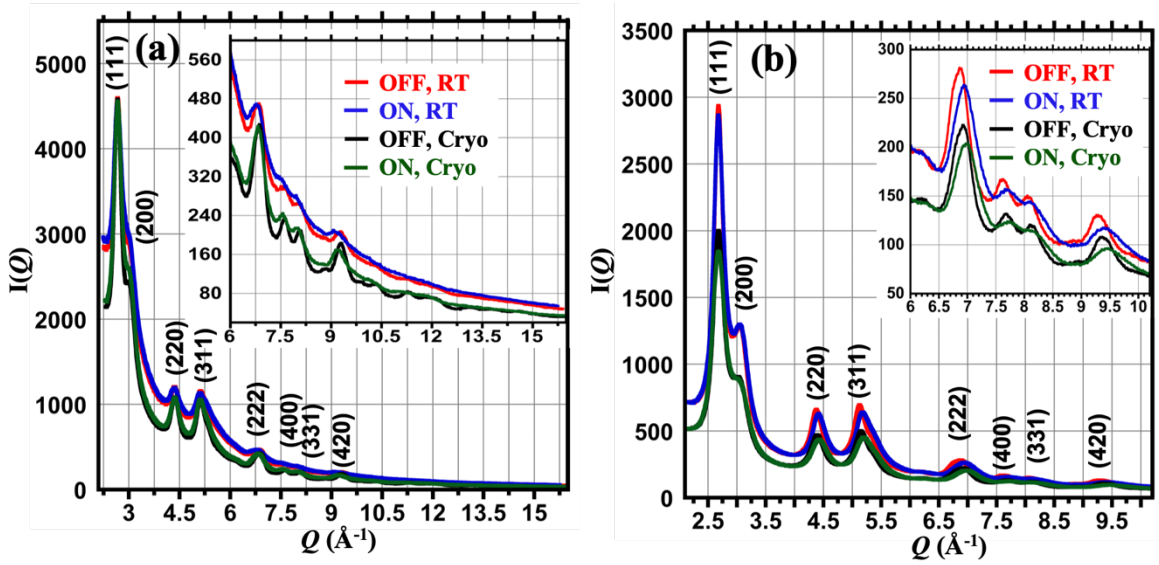


**Figure 2**. Intensity profile for (a) ~ 4.2 nm Au NPs, and (b) ~ 4.5 nm Au NPs under various conditions. Here, RT: Room temperature; liquid nitrogen temperature (Cryo), OFF: Precession OFF, ON: Precession ON. Inset showing intensity profiles in high $Q$ region. The plot in terms of scattering vector, $s = 2sin\theta/\lambda$ are presented in the Figure S1.

**Pair Distribution Function.** The pair distribution function (PDF), $G(r)$, represents the probability of finding two neighboring atoms separated by a distance $r$.[4, 38-40] Experimentally, PDFs can be obtained through the Fourier transform of a diffraction pattern. For this, the 1D intensity profile (Figure 2) is properly normalized into the total structure function, $S(Q)$, and converted to reduced structure function, $F(Q) = Q[S(Q) - 1]$. The reduced PDF, $G(r)$, is obtained as:

$$G(r) = \frac{2}{\pi}\int_{Q_{min}}^{Q_{max}} F(Q)Sin(Qr)dQ \quad (1)$$

where, $Q = 4\pi sin\theta/\lambda$, is the length of the scattering vector. For mathematical details see the references 4 and 35.

There are several software packages available to process electron diffraction data to obtain $S(Q)$ or $F(Q)$ as well as the reduced PDF, $G(r)$, and normalized PDF, $g(r)$. In this present work, the packages SUePDF and eRDF are being explored to obtain PDF data from electron diffraction. These programs calculate the proper electron scattering factors in order to normalize the intensity and also generate a model for the atomic scattering background to be subtracted from the experimental intensity. In order to have further confirmation about the quality of the $G(r)$ obtained under low temperature and precession, we used python-based program suite Diffpy-CMI to compare the obtained experimental $G(r)$ with the ideal $G(r)$ for Au. The agreement between theoretical and experimental PDFs can be measured by the least-square residual, $R_w$, written as,[4]

$$R_w = \sqrt{\frac{\Sigma_n\left(G_{experimental,n} - G_{theoretical,n}\right)^2}{\Sigma_n\, G^2_{experimental,n}}} \quad (2)$$

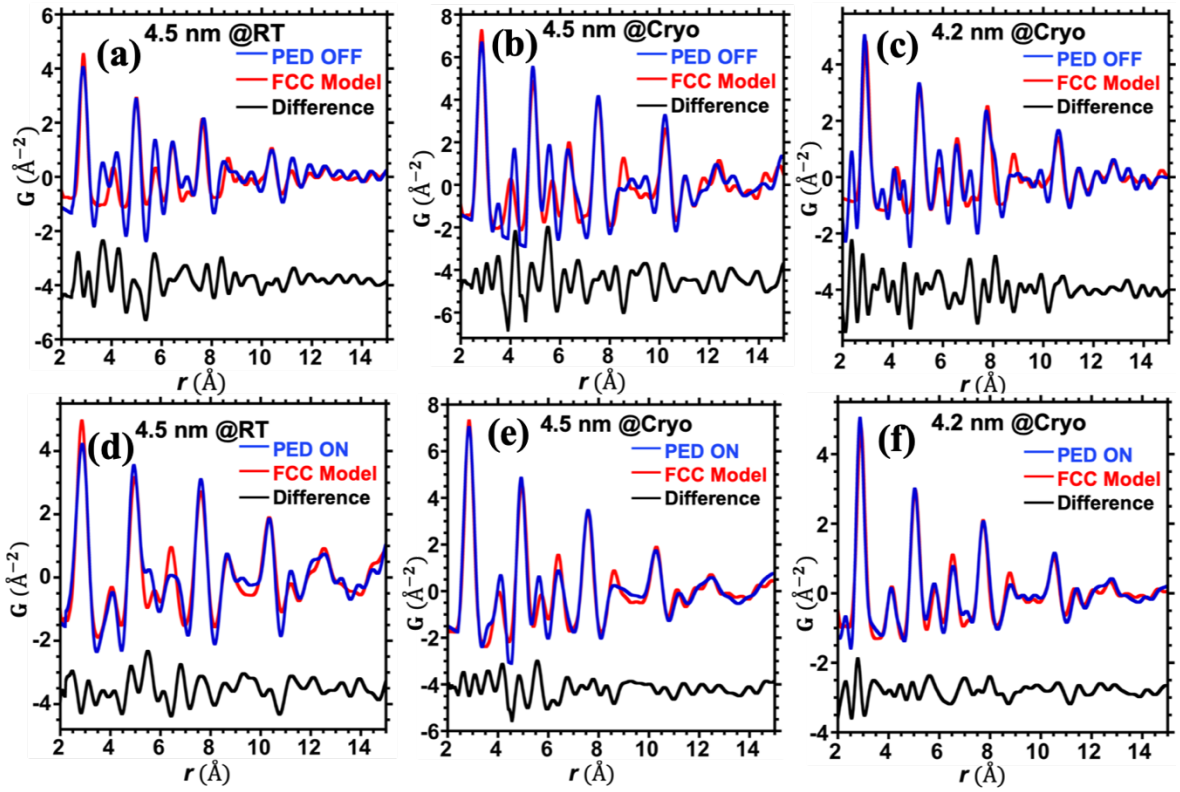


**Figure 3.** PDF fit analysis of ~ 4.5 nm Au NPs in comparison with *fcc* Au in room temperature (4.5@RT), (a) without precession ($R_w$ = 46%), and (d) with precession ($R_w$ = 29%). In cryogenic temperature (4.5@Cryo), (b) without precession ($R_w$ = 39%), and (e) with precession ($R_w$ = 23%). hexanethiolated ~ 4.2 nm Au NPs in comparison with *fcc* Au at cryogenic temperature (4.2@Cryo), (c) without precession ($R_w$ = 43%), and (f) with precession ($R_w$ = 22%). The refined parameters of these PDF fit analysis are provided in table S1 for ~ 4.5 and Table S2 for ~ 4.2 nm.

**PDF fit Analyses**. Figure 3 presents the PDF fit analyses of ~ 4.5 and 4.2 nm Au NPs using a structure-model of bulk-like *fcc* Au. $R_w$ and other important fitting parameters provided by Diffpy-CMI are summarized in Table S1 in SI section. From these analyses we have observed the improvement of $G(r)$, when low temperature and the precession electron diffraction conditions are used as observed in the Figure 3.

For the case of lipoic acid protected Au NPs, we obtained a $R_w$ of 46% when diffraction patterns were collected at room temperature, whereas precession improved this $R_w$ to 29%.

Diffpy-CMI allows variations in the isotropic atomic displacement parameters, commonly referred to the value of $U_{iso}$, permitting the displacement of atoms to optimize the PDF fit. Depending on the final reported values for $U_{iso}$, one can assess whether the fit is acceptable or not. Our $U_{iso}$ and other refined parameters (see Tables S1 and S2) are comparable with previous reports (see references 4 and 5, for example), which is a good indication that our data were not over fitted and retrieved the actual structural information.

The low temperature condition (without precession) reduced the $R_w$ from 46% to 39%, whereas the minimum residual was obtained when both low temperature and precession were combined, with a $R_w$ of 23%. In the case of the ~ 4.2 nm Au NPs, we collected electron diffraction patterns at liquid-nitrogen temperature, due to the fact that the patterns of the lipoic acid protected NPs exhibited less residual at low temperature. The residual obtained using precession and low temperature for these hexanethiolated NPs is 22%. This is indeed a good agreement with the *fcc* structure reported in a recent published article of the same sample of 400 kDa Au NPs; where the structural analysis was performed by aberration-corrected scanning transmission electron microscopy (Cs-STEM).[41] We believe that the improvement in the fitting achieved with low temperature comes from the reduction of atomic vibrations, usually corrected through the Debye-Waller approach. In this sense, the use of PED-TEM diffraction data follows the tendency in structural studies where low temperature allows a better gathering of structural parameters in diffraction (X-rays, electron, etc.) and spectroscopic methods (ex. EXAFS).

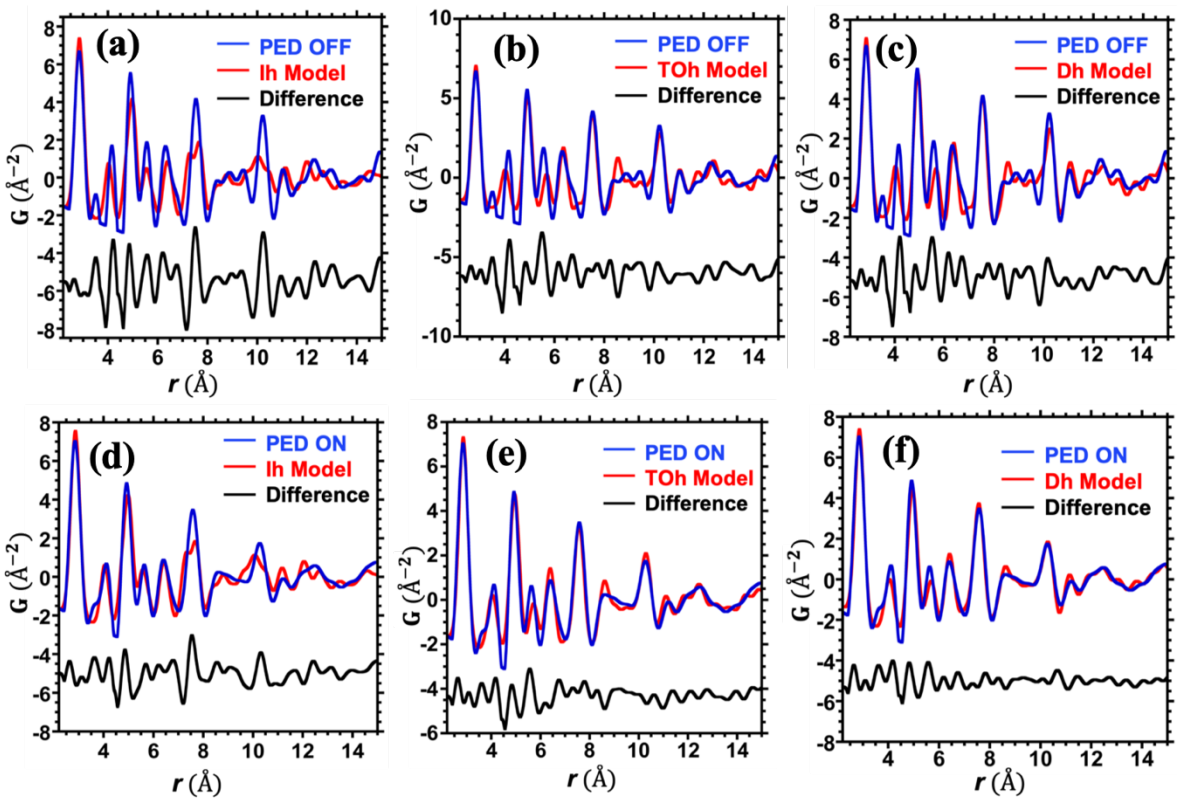


**Figure 4.** PDF fit analysis of cryo-ED results obtained on ~ 4.5 nm Au NPs, with and without precession, in comparison with different structure-models: Ih (a) PED OFF, $R_w$ = 55%, (d) PED ON, $R_w$ = 36%; TOh (b) PED OFF, $R_w$ = 39%, (e) PED ON, $R_w$ = 24%, and Dh (c) PED OFF, $R_w$ = 39%, (f) PED ON, $R_w$ = 22%. The refined parameters of these PDF fit analysis are provided in the tables S1.

For the lipoic acid protected nanoparticles, three different structures were identified in the HRTEM images: truncated octahedron (TOh), icosahedron (Ih), and decahedron (Dh) as shown in Figure S2. The structure-models for ~ 4.5 nm (no. of atoms ~ 3000) and ~ 4.2 nm (no. of atoms ~ 2000) Au NPs have been simulated using atomic simulation environment (ASE) a Python module for running and analyzing atomistic simulations;[5,42] and jmol software was used for visualization purpose. For the truncated octahedron structure-model using Wulff construction, the surface potentials are used as in Zhang *et al.*[43] Figures 4 and 5 show the PDF

fit analyses using these three different structure-models for lipoic acid and hexanethiolate protected particles, respectively.

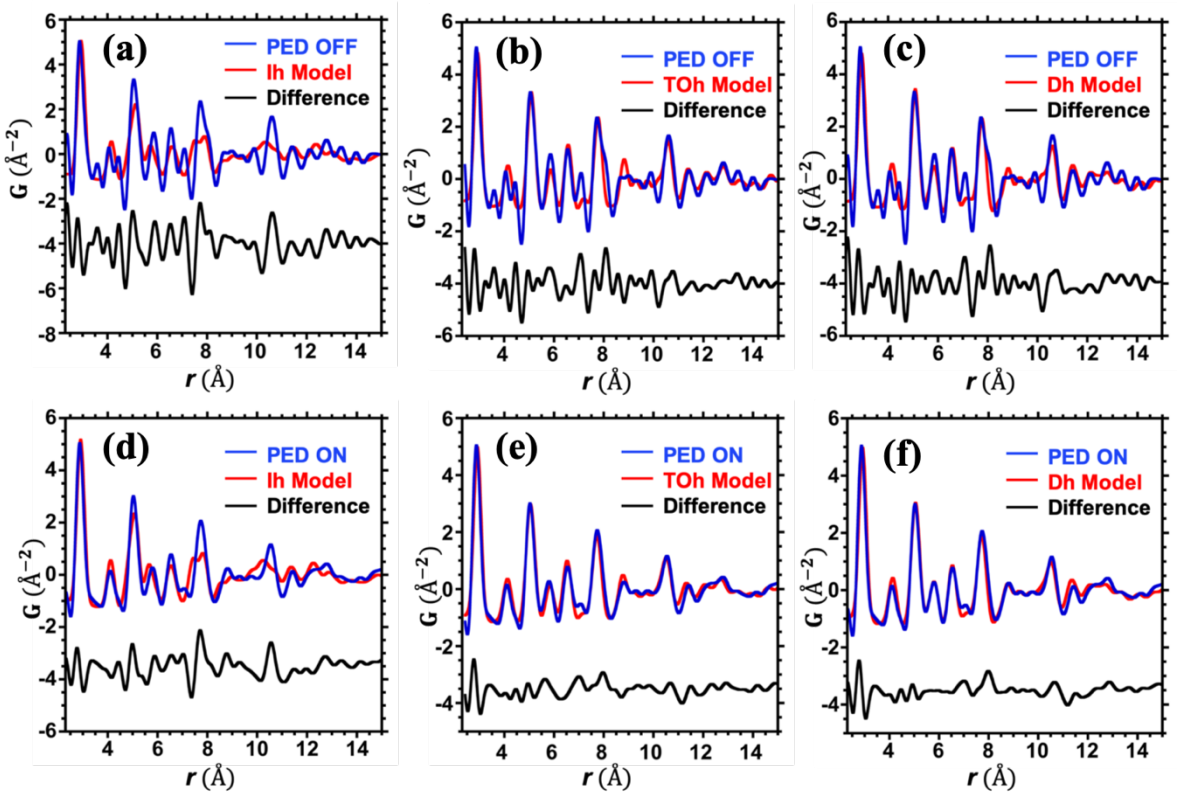


**Figure 5.** PDF fit analysis of cryo-ED results obtained on ~ 4.2 nm Au NPs with and without precession in comparison with different structure-models: Ih (a) PED OFF, $R_w$ = 62%, (c) PED ON, $R_w$ = 40%; TOh (b) PED OFF, $R_w$ = 44%, (e) PED ON, $R_w$ = 25%, and Dh (c) PED OFF, $R_w$ = 45%, (f) PED ON, $R_w$ = 25%. The PDF fit refined parameters are provided in Table S2.

When the PDF fit analyses were performed with different structure-models: it was observed that TOh and Dh model provided the best fit with a $R_w$ of 24% and 22%, respectively for the case of ~ 4.5 nm (Figures 4), and 25% for ~ 4.2 nm Au NPs (Figure 5). However, when compared with icosahedron model the $R_w$ is quite high, 40% for 4.2 and 36% for 4.5 nm Au NPs. From these analyses we speculate that in our both samples all the NPs are not having

same morphology, instead there are combination of different structures, e.g. TOh and Dh dominantly present in the sample as it is observed in the HRTEM images. The refined parameters of these PDF fit analysis are provided in the tables S1 and S2.

In a recent work Banerjee *et al*.[5] performed X-ray PDF fit analyses for various nanoparticles and nanoclusters compared with several discrete cluster models. Briefly, they performed fit analysis of Pd NPs (3.6 nm) with the *fcc* AC (attenuated crystal) model and achieved $R_w$ = 25%; but when it was compared with Dh model then the fit improved by a factor of 2, $R_w$ = 12%. On the other hand, when the fit analyses were performed for the case of $Au_{144}(SC_6)_{44}$ cluster (~ 2 nm) with the same *fcc* AC model, or with an TOh model, their residual is quite high with $R_w$ = 51%, and it is same TOh model. The residual was improved with an Ih model to $R_w$ = 29%. However, when the fit analysis was performed for the case of $Au_{146}$(p-MBA)$_{57}$, the residual improved to $R_w$ =14%, by a factor of 2. This improvement makes sense as we know that the ubiquitous $Au_{144}(SR)_{60}$ (R = benzyl) forms an icosahedron structure; thanks to the recent X-ray crystal structure determination by Yan *et al*.[44] When it was further compared with a Dh model, just as they achieved better fit in the case of Pd, it does not seem to be improved in comparison with *fcc* AC and TOh model.

In addition, the *cluster* is different than the *colloidal* Au NPs, clusters atomically precise composition (gold and thiol) is achieved.[45-46] In the case of nanoparticles, even though nowadays highly monodispersed samples have been reported,[11, 28] the size distribution of nanoparticles is far beyond the atomic precision, which may derive in higher $R_w$ values when PDF fit is done. In this context, the fit agreements, $R_w$ values obtained herein using the improved precession electron diffraction are comparable with the reported results obtained using high energy X-ray sources.[4-6]

**Coordination Numbers**. The Coordination numbers (CNs) for the peaks in the PDF were also calculated with and without precession under cryogenic conditions for ~ 4.5 nm Au NPs using process diffraction software.[32-34] In a coordination shell the number of atoms, $N(r)$, is related to the PDF as,

$$N(r) = \int_{r_1}^{r_2} 4\pi\rho_0 r^2 g(r) dr \quad (3)$$

$N(r)$ can be retrieved from the experimental $G(r)$ as,

$$N(r) = \int_{r_1}^{r_2} [4\pi\rho_0 r^2 + rG(r)] dr \quad (4)$$

In theory, the first coordination shell of bulk gold consists of 12 neighboring atoms (excluding the surface effects) at 2.88 Å. Our first experimental peak was centered at 2.85 Å; the integral (Eq. 4) corresponding to this peak resulted in a coordination number of 12.1 under precession, whereas the unprecessed case resulted in 19.6 atoms. Thus, the inclusion of the precession reduced the error from 63% to 0.8%. Figure 5 shows the trends of the improvements in the CN experimental estimation at several inter-atomic distances. For the first three inter-atomic distances (2.88, 4.08, 4.99 angstrom) the experimentally calculated CN from PDF with precession (PED ON) matches with the ideal gold CN, though with longer inter-atomic distances (5.77 and 6.45 angstrom) there is a deviation observed from the ideal CN. The Coordination numbers for spherical particles with size (diameter) ranging from 2-5 nm (249-3925 atoms) derived from a spherical volume cut directly from an *fcc* crystal (no faceting was included) are provided in the Table S3.

.

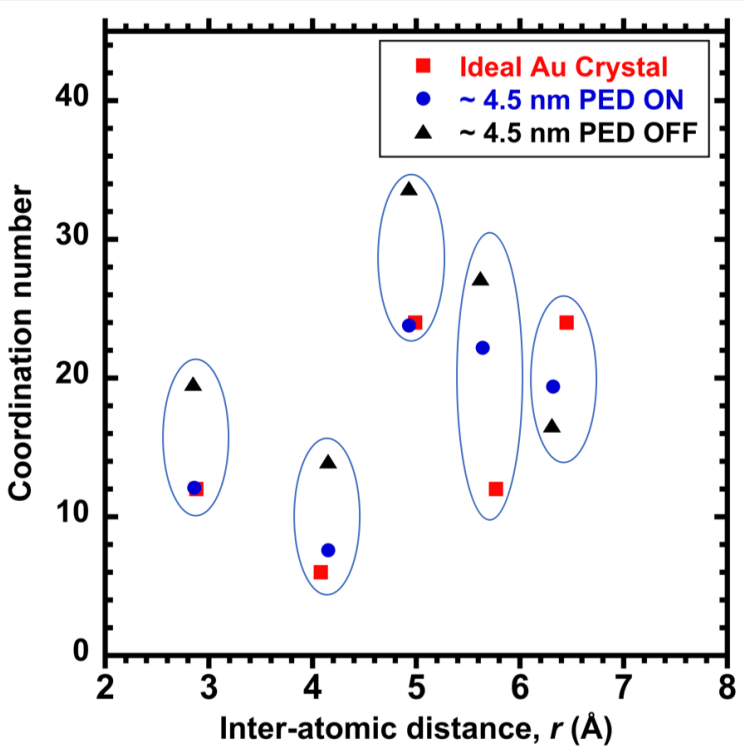


**Figure 6.** Experimentally calculated coordination number. CN calculated from data set with precession (red squares) or without precession (blue circles) is compared with theoretical coordination numbers for an ideal gold crystal (black triangle). Data points belonging to same inter-atomic distance are encircled in blue color.

**PED-PDF.** A conventional SAED pattern of nanoparticles acquired in a TEM represents the equivalent to a powder diffraction in X-rays (Debye–Scherrer patterns). The basic idea is that the intensities of the crystals are rotationally averaged (Rot-Ave). Expressing this mathematically, the powder diffraction intensities should represent:

$$I^{Rot-Ave}(g) = \int_0^{\pi}\int_0^{2\pi} d\theta d\phi \; I(g,\theta,\phi) \qquad (5)$$

Nevertheless, the SAED patterns of nanoparticles are *not* acquired by rotating a single nanocrystal. Instead, the pattern is built by the incoherent addition of single-particle patterns for an ensemble of randomly oriented particles (index *n*). In this way, we acquire a ring pattern

($I^{SAED}(g)$) by superposition of number of spot patterns ($I_n(g)$). The spot pattern for each nanoparticle includes peak broadening due to size effects and also with peak intensities that do not follow the kinematical approximation due to multiple scattering (usually described as dynamical effects). Then, an experimental SAED ring pattern represents:

$$I^{SAED}(g) = \sum_n I_n(g) \tag{6}$$

The intensities of the spot pattern of each particle $I_n(g)$ show dynamical effects, which can be significant for particles in Bragg condition; the result is a Debye–Scherrer pattern, where the intensities cannot be accounted for assuming kinematical diffraction. The occurrence of strong dynamical effects in electron Debye–Scherrer patterns for nanoparticles has already been demonstrated using the full-dynamical theory.[21] Our current study calculated the SAED intensities of Au NPs (*fcc*, icosahedral and decahedral) adding the patterns of nanoparticles in different orientations, in quite a similar procedure of how experimental patterns are obtained.

Accounting for multiple scattering and implementing a numerical procedure to correct dynamical intensities and derive kinematical ones is a very complex problem. Some simple approaches have been proposed (Blackman correction, for example); however, the applicability of this method is limited. In fact, the most advanced TEM approaches rely on comparing experimental data to time consuming dynamical simulations.

When we derive a SAED pattern using PED, we again get the incoherent superposition of single nanoparticle PED spot patterns:

$$I^{SAED+PED}(g) = \sum_n I_n^{PED}(g) \tag{7}$$

Using PED, electron diffraction spot patterns will present *"quasi-kinematical"* intensities as mentioned by Midgley and coworkers.[47] This rather ill-defined description means that PED

diffraction is not a method to invert dynamical effects and get kinematical diffraction intensities. PED diffraction intensities are something particular (neither kinematical nor dynamical), display a tendency to increase monotonically over thickness range; and if we compare the intensities among different peaks, the relative variations stay more or less constant. In other term, *"strong reflections remain strong, weak reflections remain weak"*; this fact allows the comparison of individual intensity in structural refinement methods, what has successfully contributed to a strong development of electron crystallography and determination of atomic structure.

In our present work, we have demonstrated that applying PED, we obtain *"quasi kinematical"* SAED electron diffraction patterns from nanoparticles that allow a much better PDF acquisition, as is evident by the significant reduction of residual factors.

## CONCLUSION

Combination of precession electron diffraction and low temperatures reduces the least-square residual $R_w$ with respect to electron diffraction patterns collected without precession at room temperature. The improvement of the electron diffraction patterns using PED is about 17%, and an additional 7% of the reduction is achieved at low temperatures. The superior fitting of the experimental data and structure-models are also confirmed by a better estimation of the coordination number from ePDF PED data under cryogenic conditions. Acquisition of the electron diffraction patterns using electron low dose prevents damage in the ligand-protected Au NPs and gives reproducible and consistent values.

Finally, we conclude that the cryogenic and PED measurements are an essential tool that could be used as a complementary technique to the conventional X-ray PDF methods,

especially for nanocrystals, and opens up a new door to study the structure of other types of nanostructured materials using a transmission electron microscope rather than the synchrotron X-ray sources.

## ASSOCIATED CONTENT

### Supporting Information

The Supporting Information is available free of charge on the ACS Publications website. Intensity profile in terms of scattering vector, $s = 2sin\theta/\lambda$ for ~ 4.2 nm Au NPs and ~ 4.5 nm Au NPs under various conditions. Structure-models inspired by analysis of HRTEM images of the NPs. Refined parameters from PDF fit analyses of ~ 4.5 nm Au NPs at both temperatures and ~ 4.2 nm Au NPs at cryogenic temperature. The coordination numbers derived from a spherical volume cut directly from an *fcc* crystal, and bulk-like *fcc* structure file (CIF).

## AUTHOR INFORMATION

Corresponding Author
*E-mail: Arturo Ponce (arturo.ponce@utsa.edu)

### Conflict of interest

The authors declare no competing financial interests.

## ACKNOWLEDGMENTS

Microscopy analysis was performed at the Kleberg Advanced Microscopy Center at UTSA. Authors thank the support from Department of Defense W911NF-18-1-0439 and The Welch Foundation #AX-1857, "Fundamental Chemical Research on Larger Molecular Noble Metal Clusters". C.K. and A.D. gratefully acknowledge support from NSF grant CHE-1255519. DU acknowledges financial support from CNPq (Grant. 402571/2016-9).

## REFERENCES:

(1) Hauptman, H., The direct methods of X-ray crystallography. *Science* **1986,** *233* (4760), 178-183.

(2) Hovmöller, S.; Zou, X.; Weirich, T. E. Crystal Structure Determination from EM Images. *In Advances in Imaging and Electron Physics* **2002**, *123*, 257-289.

(3) Proffen, T.; Billinge, S. J. L.; Egami, T.; Louca, D. Structural analysis of complex materials using the atomic pair distribution function—A practical guide. *Zeitschrift für Kristallographie-Crystalline Materials* **2003**, *218* (2), 132-143.

(4) Jensen, K.M.; Juhas, P.; Tofanelli, M. A.; Heinecke, C. L.; Vaughan, G.; Ackerson, C. J.; Billinge, S.J.L. Polymorphism in magic-sized Au144 (SR)60 clusters. *Nat. Commun.* **2016**, *7*, 11859.

(5) Banerjee, S.; Liu, C. H.; Lee, J. D.; Kovyakh, A.; Grasmik, V.; Prymak, O.; Koenigsmann, C.; Liu, H.; Wang, L.; Abeykoon, A. M *et al*. Improved Models for Metallic Nanoparticle Cores from Atomic Pair Distribution Function (PDF) Analysis. *J. Phys. Chem. C* **2018,** *122* (51), 29498-29506.

(6) Wu, J.; Shan, S.; Petkov, V.; Prasai, B.; Cronk, H.; Joseph, P.; Luo, J.; Zhong, C. J., Composition-Structure-Activity Relationships for Palladium-Alloyed Nanocatalysts in Oxygen Reduction Reaction: An Ex-Situ/In-Situ High Energy X-ray Diffraction Study. *Acs Catal.* **2015,** *5* (9), 5317-5327.

(7) Page, K.; Hood, T. C.; Proffen, T.; Neder, R. B., Building and refining complete nanoparticle structures with total scattering data. *J. Appl. Cryst.* **2011,** *44* (2), 327-336.

(8) Petkov, V.; Peng, Y.; Williams, G.; Huang, B.; Tomalia, D.; Ren, Y., Structure of gold nanoparticles suspended in water studied by x-ray diffraction and computer simulations. *Phys. Rev. B* **2005,** *72* (19), 195402.

(9) Petkov, V.; Shastri, S. D., Element-specific structure of materials with intrinsic disorder by high-energy resonant x-ray diffraction and differential atomic pair-distribution functions: A study of PtPd nanosized catalysts. *Phys. Rev. B* **2010,** *81* (16), 165428.

(10) Prasai, B.; Wilson, A. R.; Wiley, B. J.; Ren, Y.; Petkov, V., On the road to metallic nanoparticles by rational design: bridging the gap between atomic-level theoretical modeling and reality by total scattering experiments. *Nanoscale* **2015,** *7* (42), 17902-17922.

(11) Kumara, C., Zuo, X., Cullen, D. A., and Dass, A., Faradaurate-940- Synthesis, Mass Spectrometry, Electron Microscopy, High-Energy X-ray Diffraction, and X-ray Scattering Study of $Au_{\sim 940\pm 20}(SR)_{\sim 160\pm 4}$ Nanocrystals. *ACS Nano* **2014,** *8* (6), 6431-6439.

(12) Kumara, C.; Zuo, X.; Ilavsky, J.; Chapman, K. W.; Cullen, D. A.; Dass, A., Super-stable, highly monodisperse plasmonic Faradaurate-500 nanocrystals with 500 gold atoms: $Au_{(\sim 500)}(SR)_{(\sim 120)}$. *J. Am. Chem. Soc.* **2014,** *136* (20), 7410-7.

(13) Banerjee, S.; Liu, C. H.; Jensen, K. M. O.; Juhas, P.; Lee, J. D.; Tofanelli, M.; Ackerson, C. J.; Murray, C. B.; Billinge, S. J. L., Cluster-mining: An approach for determining core structures of metallic nanoparticles from atomic pair distribution function data. *arXiv preprint* **2019,** arXiv:1901.08754.

(14) Blackman, M., On the intensities of electron diffraction rings. *Proceedings of the Royal Society of London. Series A. Mathematical and Physical Sciences* **1939,** *173* (952), 68-82.

(15) Das, P. P.; Nicolopoulos, S.; Gemmi, M., Precession diffraction for reliable electron pair distribution function analysis. *Acta Cryst. A* **2017,** *73* (a2), C983.

(16) Avilov, A.; Kuligin, K.; Nicolopoulos, S.; Nickolskiy, M.; Boulahya, K.; Portillo, J.; Lepeshov, G.; Sobolev, B.; Collette, J. P.; Martin, N.; Robins, A. C. Fischione, P. Precession technique and electron diffractometry as new tools for crystal structure analysis and chemical bonding determination. *Ultramicroscopy* **2007**, *107* (6-7), 431-444.

(17) Vincent, R.; P.A. Midgley, Double conical beam-rocking system for measurement of integrated electron diffraction intensities. *Ultramicroscopy* **1994**, *53* (3), 271-282.

(18) Gjønnes, K. On the integration of electron diffraction intensities in the Vincent-Midgley precession technique. *Ultramicroscopy* **1997**, *69* (1), 1-11.

(19) Song, K.; Kim, Y.; Kim, Y.; Kim, J. Application of theta-scan precession electron diffraction to structure analysis of hydroxyapatite nanopowder. *J. Electron Micros.* **2011**, *61* (1), 9-15.

(20) Prodan, G.; Ciupina, V. Rietveld analysis of policrystalline materials using precession of electron diffraction. *Rom. Biotech. Lett.* **2010**, *15* (3), 103.

(21) Hall, B. D.; Ugarte, D.; Reinhard, D.; Monot, R. Calculations of the dynamic Debye–Scherrer diffraction patterns for small metal particles. *J. Chem. Phys.* **1995**, *103* (7), 2384-2394.

(22) Abeykoon, A. M. M.; Malliakas, C. D.; Juhás, P.; Bozin, E. S.; Kanatzidis, M. G.; Billinge, S. J. L. Quantitative nanostructure characterization using atomic pair distribution functions obtained from laboratory electron microscopes. *Z. Kristallogr.* **2012**, *227* (5), 248-256.

(23) Simpson, C. A.; Salleng, Kenneth J.; Cliffel, David E.; Feldheim, Daniel L. In vivo toxicity, biodistribution, and clearance of glutathione-coated gold nanoparticles. *Nanomedicine: Nanotechnology, Biology and Medicine* **2013**, *9* (2), 257-263.

(24) Goodman, C. M.; McCusker, C.D.; Yilmaz, T.; Rotello, V.M. Toxicity of gold nanoparticles functionalized with cationic and anionic side chains. *Bioconjugate Chem.* **2004**, *15* (4), 897-900.

(25) Zhang, X. D.; Wu, H. Y.; Wu, D.; Wang, Y. Y.; Chang, J. H.; Zhai, Z. B.; Meng, A. M.; Liu, P. X.; Zhang, L. A.; Fan, F. Y. Toxicologic effects of gold nanoparticles in vivo by different administration routes. *Int. J. Nanomedicine* **2010**, *5*, 771.

(26) Alkilany, A.M. C.J. Murphy, Toxicity and cellular uptake of gold nanoparticles: what we have learned so far? *J. Nanopart. Res.* **2010**, *12* (7), 2313-2333.

(27) Jin, R.; Qian, H.; Wu, Z.; Zhu, Y.; Zhu, M.; Mohanty, A.; Garg, N. Size Focusing: A Methodology for Synthesizing Atomically Precise Gold Nanoclusters. *J. Phys. Chem. Lett.* **2010**, *1* (19), 2903-2910.

(28) Kumara, C.; Hoque, M. M.; Zuo, X.; Cullen, D. A.; Whetten, R. L.; Dass, A., Isolation of a 300 kDa, $Au_{\sim 1400}$ Gold Compound, the Standard 3.6 nm Capstone to a Series of Plasmonic Nanocrystals Protected by Aliphatic-like Thiolates. *J. Phys. Chem. Lett.* **2018,** *2018* (9), 6825-6832.

(29) Ortega, E.; Ponce, A.; Santiago, U.; Alducin, D.; Benitez-Lara, A.; Plascencia-Villa, G.; José-Yacamán, M. Structural damage reduction in protected gold clusters by electron diffraction methods. *Advanced Structural and Chemical Imaging* **2017**, *2* (1), 12.

(30) Rauch, E.; M. Véron, Automated crystal orientation and phase mapping in TEM. *Mater. Charact.* **2014**, *98*, 1-9.

(31) Mitchell, D. R. G., DiffTools: Electron diffraction software tools for DigitalMicrograph. *Microsc. Res. Tech.,* **2008,** *71* (8), 588-593.

(32) Lábár, J.L. Electron Diffraction Based Analysis of Phase Fractions and Texture in Nanocrystalline Thin Films, Part I: Principles. *Microsc. Microanal.* **2008**, *14* (4), 287-295.34.

(33) Lábár, J.L. Electron diffraction based analysis of phase fractions and texture in nanocrystalline thin films, Part II: Implementation. *Microsc. Microanal.* **2009**, *15* (1), 20-29.

(34) Lábár, J.L.; Adamik, M.; Barna, B.P.; Czigány, Z.; Fogarassy, Z.; Horváth, Z.E.; Geszti, O.; Misják, F.; Morgiel, J.; Radnóczi, G. Sáfrán, G. Electron diffraction based analysis of phase fractions and texture in nanocrystalline thin films, part III: Application examples. *Microsc. Microanal.* **2012**, *18* (2), 406-420.

(35) Tran, D.T.; Svensson, G.; Tai, C. SUePDF: a program to obtain quantitative pair distribution functions from electron diffraction data. *J. Appl. Crystallogr.* **2017**, *50* (1), 304-312.

(36) Shanmugam, J.; Borisenko, K. B.; Chou, Y.; Kirkland, A. I. eRDF Analyser: An interactive GUI for electron reduced density function analysis. SoftwareX 2017, 6, 185-192.

(37) Juhás, P.; Farrow, C. L.; Yang, X.; Knox, K. R.; Billinge, S. J. L. Complex modeling: a strategy and software program for combining multiple information sources to solve ill posed structure and nanostructure inverse problems. *Acta Cryst. A* **2015**, *71* (6), 562-568.

(38) Reinhard, B.N.; Vladimir, I.K. Structure of nanoparticles from powder diffraction data using the pair distribution function. *J. Phys.: Condens. Matter* **2005**, *17* (5), S125.

(39) Farrow, C.L.; Billinge, S.J. Relationship between the atomic pair distribution function and small-angle scattering: implications for modeling of nanoparticles. *Acta Cryst. A* **2009**, *65* (3), 232-239.

(40) Billinge, S.J. Nanoscale structural order from the atomic pair distribution function (PDF): There's plenty of room in the middle. *J. Solid State Chem.* **2008**, *181* (17), 1695-1700.

(41) Vergara, S.; Santiago, U.; Kumara, C.; Alducin, D.; Whetten, R. L.; José Yacamán, M.; Dass, A.; Ponce, A. Synthesis, Mass Spectrometry and Atomic Structural Analysis of $Au_{\sim 2000}(SR)_{\sim 290}$ Nanoparticles. *J. Phys. Chem. C* **2018**, *122* (46), 26733–26738.

(42) Larsen, A.H.; Mortensen, J.J.; Blomqvist, J.; Castelli, I.E.; Christensen, R.; Dułak, M.; Friis, J.; Groves, M.N.; Hammer, B.; Hargus, C. Hermes, E.D. The atomic simulation environment—a Python library for working with atoms. *J. Phys.: Condens. Matter* **2017**, *29* (27), 273002.

(43) Zhang, J.M.; Ma, F.; Xu, K.W. Calculation of the surface energy of FCC metals with modified embedded-atom method. *Appl. Surf. Sci.* **2004**, *229* (1-4), 34-42.

(44) Yan, N.; Xia, N.; Liao, L.; Zhu, M.; Jin, F.; Jin, R.; Wu, Z., Unraveling the long-pursued $Au_{144}$ structure by x-ray crystallography. *Science advances* **2018,** *4* (10), eaat7259.

(45) Chakraborty, I. P., T., Atomically Precise Clusters of Noble Metals: Emerging Link between Atoms and Nanoparticles. *Chem. Rev.* **2017,** *117* (12), 8208-8271.

(46) Jin, R.; Zeng, C.; Zhou, M.; Chen, Y., Atomically Precise Colloidal Metal Nanoclusters and Nanoparticles: Fundamentals and Opportunities. *Chem. Rev* **2016,** *116* (18), 10346-413.

(47) Midgley, P. A.; Eggeman, A. S., Precession electron diffraction–a topical review. *IUCrJ* **2015,** *2* (1), 126-136.

## TOC Graphic